Research Article

M1-type microglia can induce astrocytes to deposit chondroitin sulfate proteoglycan after spinal cord injury

https://doi.org/10.4103/1673-5374.324858
Date of submission: April 1, 2021
Date of decision: June 29, 2021
Date of acceptance: July 29, 2021
Date of web publication: September 17, 2021

Shui-Sheng Yu#, Zi-Yu Li#, Xin-Zhong Xu, Fei Yao, Yang Luo, Yan-Chang Liu, Li Cheng*, Mei-Ge Zheng*, Jue-Hua Jing*

Graphical Abstract *Effect of M1-type microglia on astrocytes after spinal cord injury*

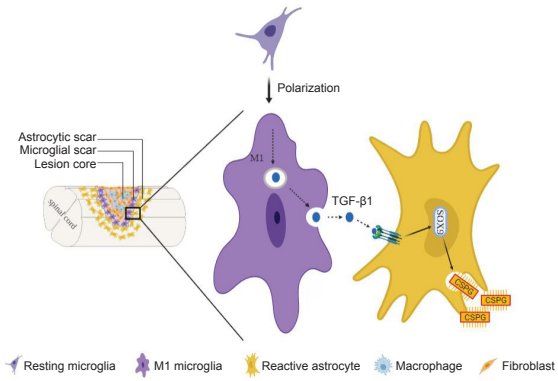

Abstract

After spinal cord injury (SCI), astrocytes gradually migrate to and surround the lesion, depositing chondroitin sulfate proteoglycan-rich extracellular matrix and forming astrocytic scar, which limits the spread of inflammation but hinders axon regeneration. Meanwhile, microglia gradually accumulate at the lesion border to form microglial scar and can polarize to generate a pro-inflammatory M1 phenotype or an anti-inflammatory M2 phenotype. However, the effect of microglia polarization on astrocytes is unclear. Here, we found that both microglia ($CX3CR1^+$) and astrocytes ($GFAP^+$) gathered at the lesion border at 14 days post-injury (dpi). The microglia accumulated along the inner border of and in direct contact with the astrocytes. M1-type microglia ($iNOS^+CX3CR1^+$) were primarily observed at 3 and 7 dpi, while M2-type microglia ($Arg1^+CX3CR1^+$) were present at larger numbers at 7 and 14 dpi. Transforming growth factor-β1 (TGFβ1) was highly expressed in M1 microglia *in vitro*, consistent with strong expression of TGFβ1 by microglia *in vivo* at 3 and 7 dpi, when they primarily exhibited an M1 phenotype. Furthermore, conditioned media from M1-type microglia induced astrocytes to secrete chondroitin sulfate proteoglycan *in vitro*. This effect was eliminated by knocking down sex-determining region Y-box 9 (SOX9) in astrocytes and could not be reversed by treatment with TGFβ1. Taken together, our results suggest that microglia undergo M1 polarization and express high levels of TGFβ1 at 3 and 7 dpi, and that M1-type microglia induce astrocytes to deposit chondroitin sulfate proteoglycan via the TGFβ1/SOX9 pathway. The study was approved by the Institutional Animal Care and Use Committee of Anhui Medical University, China (approval No. LLSC20160052) on March 1, 2016.
Key Words: astrocytes; astrocytic scar; chondroitin sulfate proteoglycan; M1/M2 polarization; microglia; sex-determining region Y-box 9; spinal cord injury; transforming growth factor-β1

Chinese Library Classification No. R446; R741; R619+.6

Introduction

Glial cells have been reported to play key roles in neuroprotection, neurodegeneration, and neuroinflammation (Amor et al., 2010; Jaerve and Müller, 2012; Joya and Martín, 2021). It is widely accepted that astrocytes play critical roles in maintaining homeostasis, regulating synaptic and neuronal function, repairing the blood-brain barrier, and alleviating neuronal injury (Bélanger and Magistretti, 2009; Cabezas et al., 2014; Allen and Eroglu, 2017). After spinal cord injury (SCI), astrocytes gradually migrate to and surround the lesion core, forming astrocytic scar (Wanner et al., 2013; Hara et al., 2017). Although astrocytic scar has beneficial effects, including limiting inflammation and promoting wound healing, it also deposits chondroitin sulfate proteoglycan (CSPG), which attenuates axon growth cone activity, significantly hindering axonal regeneration (McKeon et al., 1991, 1995; Tran et al., 2018; Alizadeh et al., 2019). Moreover, eliminating CSPG can promote SCI repair (Bradbury et al., 2002), highlighting the importance of investigating the mechanism of astrocyte-mediated CSPG deposition.

The innate microglia, which are immune cells in the central nervous system, are activated rapidly post-injury (Huang

Department of Orthopedics, The Second Hospital of Anhui Medical University, Hefei, Anhui Province, China
*Correspondence to: Jue-Hua Jing, MD, PhD, jjhhu@sina.com; Mei-Ge Zheng, PhD, zhengmg113@126.com; Li Cheng, MS, chengli7788@163.com.
https://orcid.org/0000-0001-5599-5672 (Jue-Hua Jing); https://orcid.org/0000-0002-1071-9903 (Shui-Sheng Yu)
#Both authors contributed equally to this study.

Funding: *This work was supported by the National Natural Science Foundation of China, Nos. 81801220 (to MGZ), 81671204 (to JHJ); and Key Research and Development Projects of Anhui Province of China, No. 202004j07020042 (to JHJ).*
How to cite this article: *Yu SS, Li ZY, Xu XZ, Yao F, Luo Y, Liu YC, Cheng L, Zheng MG, Jing JH (2022) M1-type microglia can induce astrocytes to deposit chondroitin sulfate proteoglycan after spinal cord injury. Neural Regen Res 17(5):1072-1079.*

and Ye, 2012; Herz et al., 2017). Recently, it was reported that microglia gradually migrate to the lesion core to form microglial scar adjacent to the inner side of astrocytic scar after SCI, and that depletion of microglia results in disruption of astrocytic scar boundary continuity and macrophage diffusion after SCI (Bellver-Landete et al., 2019), indicating that microglia play an important role in the formation and stabilization of astrocytic scar. Furthermore, the inflammatory phenotype of microglia is plastic and depends on the injury microenvironment (Sica and Mantovani, 2012). Classically activated M1-type microglia induced with lipopolysaccharide or interferon γ are associated with a pro-inflammatory response (Kroner et al., 2014; Orihuela et al., 2016), while M2-type microglia induced with interleukin-4 or interleukin-13 are associated with anti-inflammation and neuroprotection (Van Dyken and Locksley, 2013). However, the effects of M1- and M2-type microglia on CSPG secretion by astrocytes have not yet been reported.

Studies have shown that transforming growth factor-β 1 (TGFβ1) can activate TGFβ1 receptor on the surface of astrocytes to promote the secretion of CSPG (Dyck and Karimi-Abdolrezaee, 2015). Moreover, activating sex-determining region Y-box 9 (SOX9), a TGFβ1 target gene in astrocyte nuclei, can promote CSPG deposition (McKillop et al., 2013; Yuan et al., 2017). Whether microglia can regulate astrocyte-mediated CSPG deposition by secreting TGFβ1 remains unclear. We hypothesized that microglia may secrete TGFβ1, activating SOX9 in astrocytes and thereby promoting the deposition of CSPG after SCI. The aim of this study was to investigate the role of the TGFβ/SOX9 pathway in polarized microglial regulation of astrocyte CSPG secretion.

Materials and Methods

Animals

The animal experiments involved in this study were approved by the Institutional Animal Care and Use Committee of Anhui Medical University (approval No. LLSC20160052) on March 1, 2016. Owing to the lower limb paralysis and lack of bladder control evident in mice after SCI, as well as the long urinary tract of male mice, it is common for this mouse model to develop urinary tract infection (Jutzeler et al., 2019). In this study, we used fifty specific pathogen-free female C57BL/6J mice (weighing 20–25 g and aged 8–12 weeks), which were obtained from the Experimental Animal Center of Anhui Medical University (license No. SYXK (Wan) 2017-006). The mice were placed in a room with controlled temperature and humidity and a 12-hour day/night cycle, and had free access to water and food. All experiments were designed and reported in accordance with the Animal Research: Reporting of *In Vivo* Experiments (ARRIVE) guidelines.

Spinal cord injury model

The mice were anesthetized by intraperitoneal injection of 2% pentobarbital sodium (P-010; Sigma, St. Louis, MO, USA) and placed in the prone position. The back was then shaved at the T10 level, and the skin was disinfected with iodophor. Bone forceps were used to remove the lamina to expose the spinal cord at the T10 level, and Dumont forceps with a 0.5-mm-wide tip (No. 5, 11252-20, Fine Science Tools, Heidelberg, Germany) were used to completely compress the spinal cord from both sides for 5 seconds, resulting in moderate compression injury (Wanner et al., 2013). After the SCI was induced, the bladder was pressed twice a day to assist mice in urinating until their urination reflex recovered. Before SCI induction, the mice were randomly divided into four groups: pre-injury (n = 8) and 3 (acute phase, n = 14), 7 (subacute phase, n = 14), and 14 (subacute phase, n = 14) dpi. The total number of animals used in this study was 50. Three mice died due to intraoperative blood loss.

Cell culture and transfection

The BV-2 microglia cell line was obtained from The Rio de Janeiro Cell Bank (Cat# 0356, RRID:CVCL_0182, BCRJ, Rio de Janeiro, Brazil), and the C8-D1A astrocyte cell line was obtained from the American Type Culture Collection (CRL-2541, RRID:CVCL_6379, ATCC, Manassas, VA, USA). The C8-D1A clonal cell line, which has astrocyte characteristics, was established from postnatal day 8 mouse cerebellum cells that spontaneously transformed *in vitro* (Alliot and Pessac, 1984). Both cell lines were cultured in Dulbecco's modified Eagle medium (Cat# SH30021, HyClone, Logan, UT, USA) containing 10% fetal bovine serum (Cat# 10270106, Gibco, Grand Island, NY, USA), 100 U/mL penicillin, and 100 g/mL of streptomycin (Gibco). Cells were incubated at 5% CO_2, 95% O_2 and 37°C. A jetPRIME kit (Cat# 114-15, Polyplus Transfection, Illkirch, France) was used to transfect small interfering RNA (siRNA) into C8-D1A astrocytes in accordance with the manufacturer's instructions. A nonspecific control siRNA (NC) and an siRNA targeting mouse SOX9 (siRNA: 5′-GCA GCA CAA GAA AGA CCA CTT-3′) were obtained from GenePharma (Shanghai, China).

Microglial polarization

The BV-2 cells were inoculated at a density of 1×10^6 cells/mL into six-well plates coated with poly-D-lysine (Cat# P7280, Sigma) and cultured overnight. After 24 hours of serum deprivation, BV-2 cells were treated with phosphate-buffered saline to induce M0 polarization, lipopolysaccharide (100 ng/mL, Beyotime Biotechnology, Shanghai, China) and IFNγ (20 ng/mL, Beyotime Biotechnology) to induce M1 polarization, or IL-4 (20 ng/mL, Beyotime Biotechnology) to induce M2 polarization and cultured for 24 hours (Miron et al., 2013). Immunocytochemistry and western blotting for the M1 polarization marker inducible nitric oxide synthase (iNOS) and the M2 polarization marker arginine 1 (Arg1) were performed to confirm the microglial polarization.

Culturing astrocyte cells in microglia-conditioned medium

After the microglia had been incubated in polarization-inducing media for 24 hours, they were then cultured in Dulbecco's modified Eagle medium for another 24 hours, and the resulting supernatants were removed for use as M0-, M1-, and M2-type microglia-conditioned media (CM0, CM1, and CM2, respectively). Astrocytes were treated with microglia-conditioned medium *in vitro*. As a positive control, TGFβ1 (100 pg/mL, Cat# CK33, Novoprotein, Shanghai, China) was added to the astrocyte culture medium to promote CSPG production.

Tissue processing

For molecular analyses, mice were anesthetized with 2% pentobarbital sodium, and the blood was removed by transcardial perfusion with 0.1 M phosphate-buffered saline. A 5-mm segment of spinal cord tissue that surrounded the injury site was harvested and used for western blotting, as described below. For histological analysis, the blood was removed as described above, followed by perfusion with 4% paraformaldehyde, and a 5-mm section of the injured spinal cord was harvested as described above. The spinal cord segment was then embedded in paraffin, 6-μm sagittal sections were taken using a microtome (RM2235, Leica, Nussloch, Germany), and every tenth section was mounted for microscopic analysis.

Immunofluorescence analysis

Immunohistochemistry

The paraffin-embedded spinal cord tissues were sectioned, and sections were dewaxed by conventional methods then heated for 10 minutes at 92–98°C in citrate solution (pH 6.0) and left to cool to room temperature. Next, the sections were blocked with 10% donkey serum albumin (Cat# SL050, Solarbio, Beijing, China) containing 0.3% Triton X-100 (Solarbio,

Cat# T8200) for 1 hour at room temperature. The samples were incubated with primary antibodies at 4°C overnight. The primary antibodies used to stain the sections were as follows: rabbit anti-C-X3-C motif chemokine receptor 1 (CX3CR1, 1:500, Abcam, Cat# ab8021, RRID:AB_306203), goat anti-platelet-derived growth factor receptor β (PDGFRβ, 1:40, R&D Systems, Minneapolis, MN, USA, Cat# AF1042, RRID:AB_2162633), rat anti-glial fibrillary acidic protein (GFAP, 1:100, Invitrogen, Carlsbad, CA, USA, Cat# 13-0300, RRID:AB_2532994), rabbit anti-TGFβ1 (1:100, Affinity, Changzhou, China, Cat# AF1027, RRID:AB_2835389), rabbit anti-iNOS (1:100, Affinity, Cat# AF0199, RRID:AB_2833391), mouse anti-iNOS (1:50, Santa Cruz Biotechnology, Santa Cruz, CA, USA, Cat# sc-7271, RRID:AB_627810), mouse anti-Arg1 (1:50, Santa Cruz Biotechnology, Cat# sc-271430, RRID:AB_10648473), rabbit anti-SOX9 (1:100, Abcam, Cat# ab185966, RRID:AB_2728660), and mouse anti-CSPG (1:100, Sigma, Cat# C8035, clone CS56, RRID:AB_476879). The samples were incubated with secondary antibodies at room temperature for 1 hour. The secondary antibodies used were as follows: Alexa Fluor 594 and Alexa Fluor 488 (1:500, Invitrogen, Cat# A-21206, RRID:AB_2535792, Cat# A-21202, RRID:AB_141607, Cat# A-21203, RRID:AB_141633, Cat# A-21207, RRID:AB_141637, Cat# A-11058, RRID:AB_2534105). 4',6-Diamidino-2-phenylindole, dihydrochloride (1 μg/mL, Thermo Fisher Scientific, Waltham, MA, USA) was used for nuclear staining. Normal mouse IgG (1:100, Sigma, Cat# NI03, RRID:AB_490557) was used as a negative control for the mouse antibodies to verify the specificity of the positive staining. An Axio Scope A1 microscope (Zeiss, Oberkochen, Germany) was used to obtain fluorescence signals, and all images were compared and processed at the same light intensity. Quantitative analysis was performed using ImageJ (v1.53c, National Institutes of Health, Bethesda, MD, USA).

Immunocytochemistry

The cells were fixed in 4% paraformaldehyde for 10 minutes and blocked with 5% donkey serum albumin at room temperature for 30 minutes. They were then incubated with the primary antibodies listed in the Immunohistochemistry section above at 4°C overnight.

Imaging analysis and quantification

Five sections spanning the entire length of the injured spinal cord segment (every tenth 6-μm-thick paraffin-embedded section) were quantified for each animal. Using Zeiss ZEN imaging software (Zeiss) and a 20× objective, the total number of $CX3CR1^+$, $iNOS^+$, $Arg1^+$, $GFAP^+$, $CS56^+$, and double-positive cells was counted in each sagittal section of the spinal cord. To maintain consistency among the different stains, the fluorescence intensity γ value was fixed at 1, and the same exposure time was used for each image.

Western blot analysis

Radioimmunoprecipitation lysate (Sigma, Cat# R0278) containing phosphatase inhibitors (Roche, Mannheim, Germany, Cat# 04906845001) and protease inhibitors (Roche, Cat# 04693124001) was used to homogenize tissues. The cells were washed with cold phosphate-buffered saline twice, after which radioimmunoprecipitation lysate was added and the mixture was incubated for 30 minutes on ice and centrifuged at 4°C to obtain the supernatant. The protein extracts were quantified using an enhanced bicinchoninic acid protein assay kit (Beyotime Biotechnology, Cat# P0010S). The protein samples were separated on dodecyl sulfate-polyacrylamide gels and transferred to polyvinylidene membranes. The membranes were blocked at room temperature with 5% nonfat milk for 1 hour, then incubated with the following primary antibodies at 4°C overnight: mouse anti-β-actin (1:5000, Proteintech, Wuhan, China, Cat# 66009-1-Ig, RRID:AB_2687938), rabbit anti-TGFβ1 (1:100, Affinity, Cat# AF1027, RRID:AB_2835389), rabbit anti-iNOS (1:100, Affinity, Cat# AF0199, RRID:AB_2833391), mouse anti-Arg1 (1:50, Santa Cruz Biotechnology, Cat# sc-271430, RRID:AB_10648473), rabbit anti-SOX9 (1:100, Abcam, Cat# ab185966, RRID:AB_2728660), and mouse anti-CSPG (1:100, Sigma, Cat# C8035, clone CS56, RRID:AB_476879). The cells were then incubated with a horseradish peroxidase-conjugated goat anti-mouse secondary antibody (1:10,000, Sigma, Cat# A4416, RRID:AB_258167) or a horseradish peroxidase-conjugated goat anti-rabbit secondary antibody (1:10,000, Sigma, Cat# A0545, RRID:AB_257896) at room temperature for 1 hour. The protein bands were then visualized using a chemiluminescence detection kit (Thermo Fisher Scientific) and a Tanon 5200 system (Tanon, Shanghai, China). Quantification was performed via ImageJ, and protein expression was normalized to β-actin.

Statistical analysis

At least three independent replicates were performed for each experiment, and quantification was performed on blinded samples. All data are presented as mean ± standard error of the mean (SEM), and statistical analysis was performed using SPSS version 23.0 (IBM, Armonk, NY, USA). Differences among multiple groups were compared using one-way analysis of variance followed by Tukey's *post hoc* test. $P < 0.05$ indicated that the difference was statistically significant.

Results

Microglia and astrocytes are located adjacent to each other in the injured region after spinal cord injury

To understand the spatiotemporal distribution of astrocytes and microglia after SCI, immunofluorescence was performed to detect the relationship between microglia and astrocytes pre-injury and 3–14 dpi. After SCI, microglia and astrocytes gradually migrated to the edge of the lesion core. At 14 dpi, microglia ($CX3CR1^+$) and astrocytes ($GFAP^+$) gathered at the lesion border (**Figure 1A**). Microglia were closely adjacent to the astrocytes in the penumbra (**Figure 1B**). These findings suggest that there may be crosstalk between astrocytes and microglia during glial scar formation.

Microglia are primarily M1-type at 3 and 7 days post-injury

Microglial polarization is an important event that occurs at the injured site after SCI (David and Kroner, 2011). To understand the effect of microglial polarization on astrocytes, we detected the polarized state of microglia pre-injury and 3–14 dpi. As shown in **Figure 2A** and **B**, M1-type microglia ($iNOS^+CX3CR1^+$) were significantly increased at 3 and 7 dpi ($P < 0.0001$, *vs*. pre-injury), and decreased at 14 dpi ($P < 0.0001$, *vs*. 3 and 7 dpi). The percentages of $iNOS^+CX3CR1^+$ cells at 3 and 7 dpi relative to the total number of $CX3CR1^+$ cells in the injured spinal cord were 54.3 ± 4.4% and 76.7 ± 3.6%, respectively (**Figure 2B**). As both M1-type microglia and macrophages express iNOS (David and Kroner, 2011), we also counted iNOS+CX3CR1- cells to determine the number of M1-type macrophages and found that they were increased at 14 dpi ($P < 0.0001$, *vs*. pre-injury, 3 and 7 dpi; **Figure 2C**). $Arg1^+$ cells began to appear at 3 dpi and increased significantly at 7 and 14 dpi ($P < 0.01$ or $P < 0.001$, *vs*. pre-injury and 3 dpi, respectively; **Figure 2D** and **E**). The percentages of $Arg1^+CX3CR1^+$ cells at 7 and 14 dpi relative to the total number of $CX3CR1^+$ cells in the injured spinal cord were 16.6 ± 3.5% and 24.9 ± 2.8%, respectively (**Figure 2E**). The number of $Arg1^+CX3CR1^-$ cells (M2-type macrophages) (Wang et al., 2015) reached a peak at 7 dpi and decreased significantly at 14 dpi ($P < 0.05$, *vs*. 7 dpi; **Figure 2F**). The trends that we observed in macrophage polarization are consistent with those reported in a previous study (Kigerl et al., 2009; Wang et al., 2015). Therefore, the microglia present

at sites of SCI at 3–7 dpi are primarily M1-type.

Production of CSPG by astrocytes increases gradually after spinal cord injury

To evaluate the changes in CSPG production by astrocytes after SCI, we used an anti-CSPG antibody (CS56) to detect the spatiotemporal distribution of CSPG pre-injury and 3–14 dpi. CSPG was primarily secreted by astrocytes, and gradually increased after SCI (**Figure 3A** and **B**). At 14 dpi, astrocytes were located around the border of the lesion core, and this is where CSPG was deposited as well (**Figure 3A**). These results indicated that CSPG secretion by astrocytes gradually increased after SCI.

Microglia exhibit high TGFβ1 immunopositivity at 3 and 7 days post-injury

To explore the reasons for the increased CSPG secretion, we detected expression of TGFβ1, which has been shown to regulate CSPG production (Dyck and Karimi-Abdolrezaee, 2015), in microglia pre-injury and 3–14 dpi by immunofluorescence. There were no TGFβ1-immunopositive microglia prior to SCI, but $TGF\beta1^{+}CX3CR1^{+}$ microglia were increased at 3 and 7 dpi ($P < 0.0001$, *vs*. pre-injury and 14 dpi; **Figure 4A** and **B**). The percentages of $TGF\beta1^{+}CX3CR1^{+}$ cells at 3 and 7 dpi relative to the total number of $CX3CR1^{+}$ cells in the injured spinal cord were 34 ± 1.1% and 51.3 ± 2.4%, respectively (**Figure 4B**). These findings correspond with our earlier observation of microglial M1 polarization at 3 and 7 dpi (**Figure 2A**). Taken together, these data suggest that M1-type microglia express high levels of TGFβ1 after SCI.

TGFβ1 is highly expressed in M1-type microglia *in vitro*

Next, we observed the expression of TGFβ1 by microglia subjected to *in vitro* polarization. The western blotting results showed that treatment of BV-2 cells with lipopolysaccharide and IFNγ significantly induced expression of iNOS ($P < 0.0001$, *vs*. M0 and M2), a marker of M1 polarization (David and Kroner, 2011; Hu et al., 2015), while treatment with IL-4 significantly increased expression of Arg1 ($P < 0.001$, *vs*. M0 and M1), a marker of M2 polarization marker (David and Kroner, 2011; Hu et al., 2015), indicating that polarization was successfully induced (**Figure 5A–C**). Western blotting (**Figure 5A** and **D**) and immunocytochemistry (**Figure 5E**) indicated that TGFβ1 expression was significantly increased in M1-type microglia ($P < 0.0001$, *vs*. M0 and M2), suggesting that TGFβ1 is highly expressed by M1-type microglia.

Conditioned media from M1-type microglia promote CSPG secretion by astrocytes

To assess the effect of microglial polarization on astrocytes, we treated astrocytes with conditioned media from polarized microglia. Western blot (**Figure 6A** and **B**) and immunocytochemistry (**Figure 6C**) analyses showed that CM1 up-regulated CSPG expression by astrocytes ($P < 0.01$, *vs*. CM0 and CM2). Moreover, western blotting (**Figure 6A** and **D**) and immunocytochemistry (**Figure 6E**) showed that CM1 also promoted SOX9 expression in astrocytes ($P < 0.01$, *vs*. CM0 and CM2). These results suggested that M1-type microglia could promote astrocyte-mediated CSPG production.

M1-type microglia promote astrocyte-mediated CSPG secretion via the TGFβ1/SOX9 pathway

To determine the signaling pathway involved in M1-type microglia-induced CSPG secretion by astrocytes, we used siRNA to knock down SOX9 expression in astrocytes *in vitro*. Western blotting showed that CSPG production and SOX9 expression decreased after siSOX9 transfection ($P < 0.01$ or $P < 0.05$, *vs*. CM0, respectively), indicating that SOX9 knockdown was effective. CSPG production and SOX9 expression increased in astrocytes treated with CM1 ($P < 0.001$, *vs*. CM0), but decreased when SOX9 expression was knocked down ($P < 0.0001$, *vs*. CM1; **Figure 7**). In astrocytes treated with TGFβ1, CSPG production and SOX9 expression increased ($P < 0.0001$, $P < 0.001$, *vs*. CM0, respectively), but when SOX9 was knocked down, CSPG production and SOX9 expression declined even with TGFβ1 treatment ($P < 0.0001$, *vs*. CM0 + TGFβ1; **Figure 7**). These results showed that M1-type microglia express high levels of TGFβ1 and activate SOX9 expression in astrocytes, thus promoting CSPG production.

Discussion

Astrocytes, as the main components of glial scar after SCI, have been the focus of considerable research in recent years. Although astrocytic scar helps limit inflammation and promote wound healing after SCI, it also deposits CSPG, which significantly hinders axonal regeneration. It is widely accepted that inhibiting CSPG deposition can promote axonal regeneration after SCI, highlighting the importance of investigating the mechanism of CSPG deposition (Dyck and Karimi-Abdolrezaee, 2015; Lang et al., 2015). In the present study, we found that microglia were located along the inner border of accumulated astrocytes after SCI, indicating that there may be crosstalk between microglia and astrocytes. At 3 and 7 dpi, microglia were primarily M1-type and expressed high levels of TGFβ1, consistent with *in vitro* results showing that M1-type microglia expressed high levels of TGFβ1. CM1 induced astrocytes to produce large amount of CSPG by activating SOX9, while SOX9 knockdown in astrocytes resulted in inhibition of CSPG secretion. Therefore, we propose that M1-type microglia promote astrocyte-mediated deposition of CSPG via the TGFβ1/SOX9 pathway after SCI.

During the subacute period of SCI (7–14 dpi), activated astrocytes gradually gather at and surround the lesion core, adhering to each other and overlapping to form a barrier structure called astrocytic scar (Okada et al., 2006). Although astrocytic scar has neuroprotective effects, including inhibiting inflammation and promoting tissue retention, it also deposits CSPG, which inhibits axonal regeneration and functional recovery. CSPG is composed of a protein core and varying glycosaminoglycans, primarily neurocan, versican, brevican, and NG2; its deposition peaks at 14 dpi and persists throughout the chronic stage of SCI (Tran et al., 2018). The protein tyrosine phosphatase sigma transmembrane receptor expressed on the surface of the axon growth cone monomerizes upon contact with CSPG glycosaminoglycan fragments, leading to growth cone dystrophy and failure of axonal regeneration (Shen et al., 2009). It has been shown that inhibiting CSPG deposition can promote axonal regeneration, suggesting that inhibition of CSPG deposition after SCI may have therapeutic value (Faulkner et al., 2004; Anderson et al., 2018). A recent study showed that microglia can form another type of scar, referred to as microglial scar, after SCI. At 4–14 dpi, microglia proliferated extensively and gradually migrated to the edge of the lesion core, forming microglial scar along the inner side of astrocytic scar (Bellver-Landete et al., 2019). When spinal cord microglia were eliminated by treatment with PLX5622, a colony stimulating factor 1 receptor inhibitor (Elmore et al., 2014), astrocytic scar lost its compactness, and the inflammatory cells in the lesion core spread, leading to the deterioration of motor function in mice. Therefore, microglial scar may be involved in astrocytic scar formation after SCI, and could limit inflammation and promote wound healing and neurological recovery (Bellver-Landete et al., 2019). Our results confirm that microglia and astrocytes gathered at the lesion border at 14 dpi, and that microglia were located in close proximity to astrocytes. However, it remains unclear whether there is crosstalk between microglia and astrocytes, which could have implications for SCI treatment.

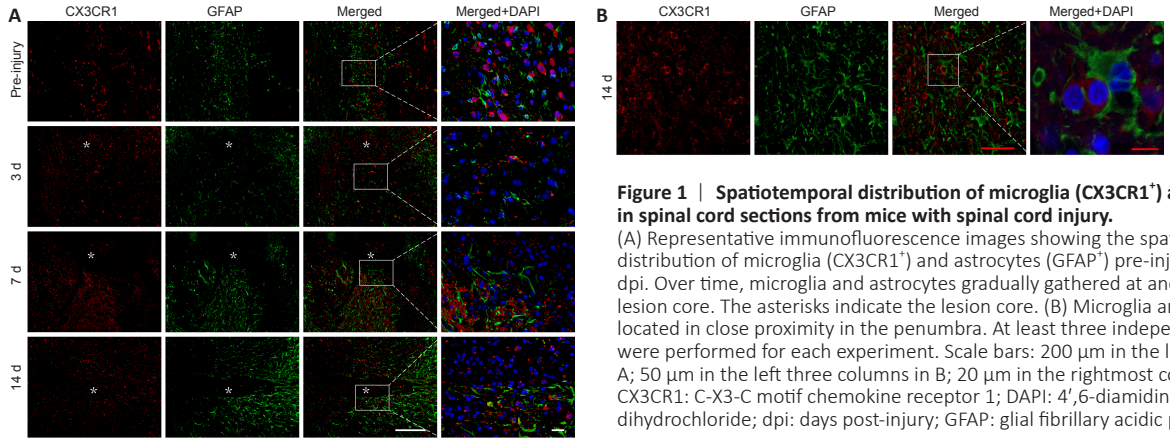

Figure 1 | Spatiotemporal distribution of microglia (CX3CR1$^+$) and astrocytes (GFAP$^+$) in spinal cord sections from mice with spinal cord injury.
(A) Representative immunofluorescence images showing the spatiotemporal distribution of microglia (CX3CR1$^+$) and astrocytes (GFAP$^+$) pre-injury and 3, 7, and 14 dpi. Over time, microglia and astrocytes gradually gathered at and surrounded the lesion core. The asterisks indicate the lesion core. (B) Microglia and astrocyte were located in close proximity in the penumbra. At least three independent replicates were performed for each experiment. Scale bars: 200 μm in the left three columns in A; 50 μm in the left three columns in B; 20 μm in the rightmost columns in A and B. CX3CR1: C-X3-C motif chemokine receptor 1; DAPI: 4′,6-diamidino-2-phenylindole, dihydrochloride; dpi: days post-injury; GFAP: glial fibrillary acidic protein.

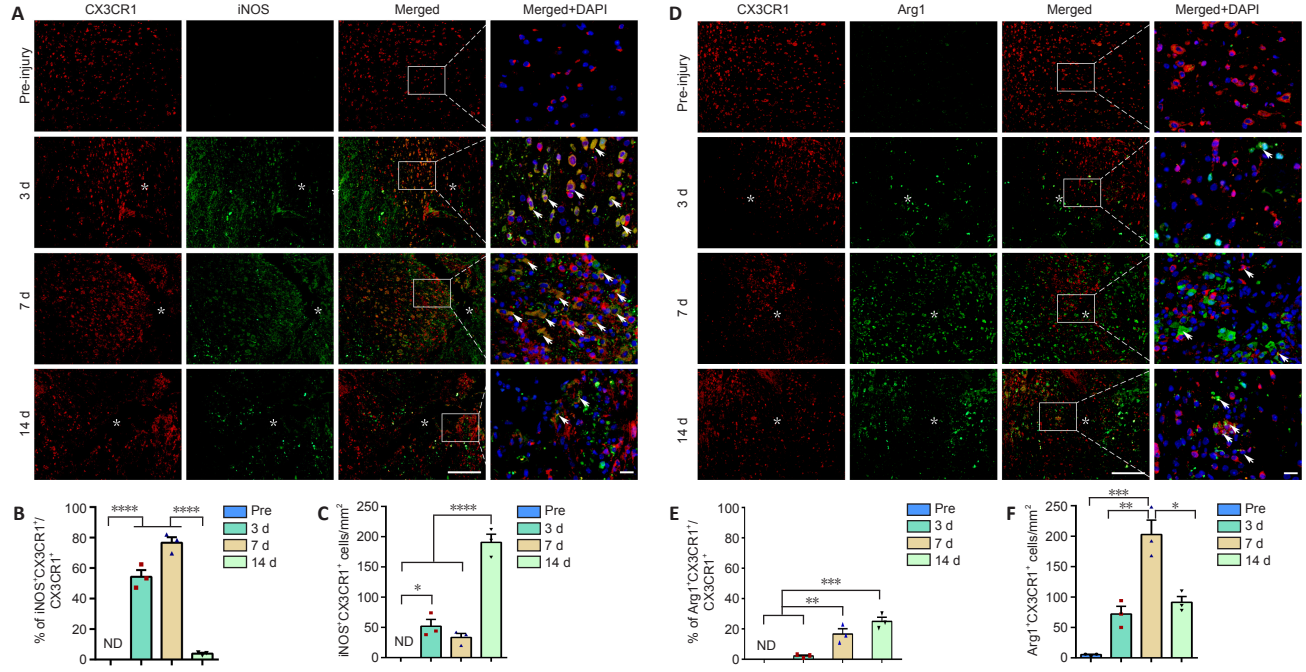

Figure 2 | Microglial polarization in spinal cord sections from mice with spinal cord injury.
(A) Representative immunofluorescence images showing the spatiotemporal distribution of CX3CR1 (red, stained with Alexa Fluor 594) and iNOS (green, stained with Alexa Fluor 488) pre-injury and 3, 7, and 14 dpi. CX3CR1$^+$ microglia were mainly M1-type at 3 and 7 dpi. Colocalization of the proteins is shown in yellow. Nuclear staining (DAPI) is shown in blue, and white arrowheads indicate the colocalization observed with a 40× objective. (B) Percentage of iNOS$^+$CX3CR1$^+$ cells relative to the total number of CX3CR1$^+$ cells in the injured spinal cord. (C) Quantification of the number of iNOS$^+$CX3CR1$^-$ cells in the injured spinal cord. (D) Representative immunofluorescence images showing the spatiotemporal distribution of CX3CR1 (red, stained with Alexa Fluor 594) and Arg1 (green, stained by Alexa Fluor 488) pre-injury and 3, 7, and 14 dpi. The highest number of Arg1$^+$CX3CR1$^-$ macrophages was seen at 7 dpi. Colocalization of the proteins is shown in yellow. Nuclear staining (DAPI) is shown in blue, and white arrowheads indicate the colocalization observed with a 40× objective. Scale bars: 200 μm in the left three columns in A and D; 20 μm in the rightmost columns in A and D. (E) Percentage of Arg1$^+$CX3CR1$^+$ cells relative to the total number of CX3CR1$^+$ cells in the injured spinal cord. (F) Quantification of Arg1$^+$CX3CR1$^-$ cells in the injured spinal cord. The data are presented as mean ± SEM (n = 3 independent experiments) and were analyzed by one-way analysis of variance, followed by Tukey's *post hoc* test. At least three independent replicates were performed for each experiment. *P < 0.05, **P < 0.01, ***P < 0.001, ****P < 0.0001. Arg1: Arginine 1; CX3CR1: C-X3-C motif chemokine receptor 1; DAPI: 4′,6-diamidino-2-phenylindole, dihydrochloride; dpi: days post-injury; GFAP: glial fibrillary acidic protein; iNOS: inducible nitric oxide synthase; ND: not determined; Pre: pre-injury.

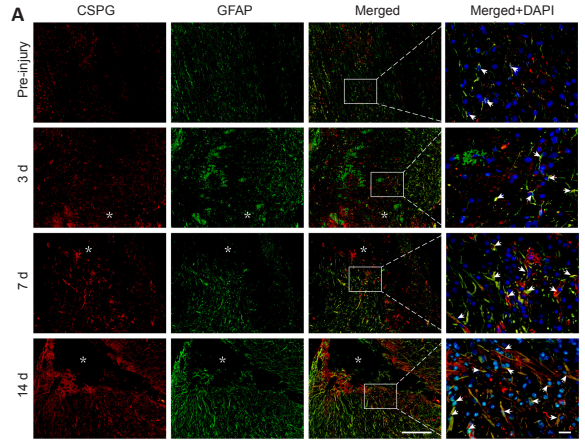

Figure 3 | CSPG secreted by astrocytes in the spinal cord of mice with spinal cord injury.
(A) Representative immunofluorescence images showing the spatiotemporal distribution of CSPG (red, stained with Alexa Fluor 594) and GFAP (green, stained with Alexa Fluor 488) pre-injury and 3, 7, and 14 dpi. GFAP$^+$ astrocytes gradually gathered at and surrounded the lesion core from 3 dpi to 14 dpi, while CSPG deposition colocalized with GFAP around the lesion core and increased significantly from 7 to 14 dpi. Colocalization of the proteins is shown in yellow. Nuclear staining (DAPI) is shown in blue, and white arrowheads indicate the colocalization observed with a 40× objective. The asterisks indicate the lesion epicenter. Scale bars: 200 μm in the left three columns; 20 μm in the right column. (B) Quantification of CSPG$^+$GFAP$^+$ cells in the injured spinal cord. The data are presented as mean ± SEM (n = 3 per group). **P < 0.001, ***P < 0.001, ****P < 0.0001 (one-way analysis of variance followed by Tukey's *post hoc* test). CSPG: Chondroitin sulfate proteoglycan; DAPI: 4′,6-diamidino-2-phenylindole, dihydrochloride; dpi: days post-injury; GFAP: glial fibrillary acidic protein.

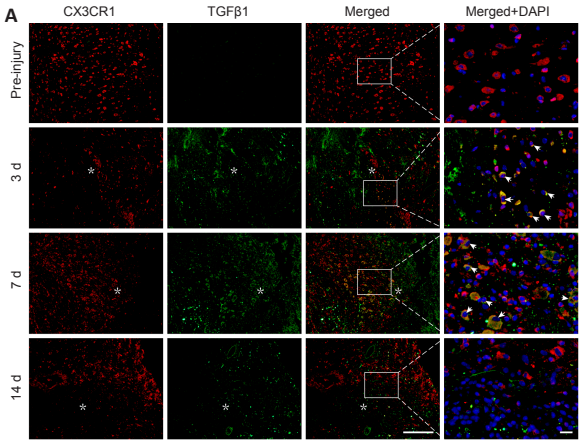

Figure 4 | TGFβ1 immunopositivity of microglia in the spinal cord of mice with spinal cord injury.
(A) CX3CR1 (red, stained with Alexa Fluor 594) and TGFβ1 (green, stained with Alexa Fluor 488) double labeling. TGFβ1 colocalized with CX3CR1 at 3 and 7 dpi, but not pre-injury or at 14 dpi. The asterisks indicate the lesion epicenter. Colocalization of the proteins is shown in yellow. Nuclear staining (DAPI) is shown in blue, and white arrowheads indicate the colocalization observed with a 40× objective. Scale bars: 200 μm in the left three columns; 20 μm in the right column. (B) Percentage of TGFβ1$^+$CX3CR1$^+$ cells relative to the total number of CX3CR1$^+$ cells in the injured spinal cord. The data are presented as the mean ± SEM (n = 3 independent experiments). ****P < 0.0001 (one-way analysis of variance followed by Tukey's *post hoc* test). CX3CR1: C-X3-C motif chemokine receptor 1; DAPI: 4′,6-diamidino-2-phenylindole, dihydrochloride; dpi: days post-injury; ND: not determined; TGFβ1: transforming growth factor-β1.

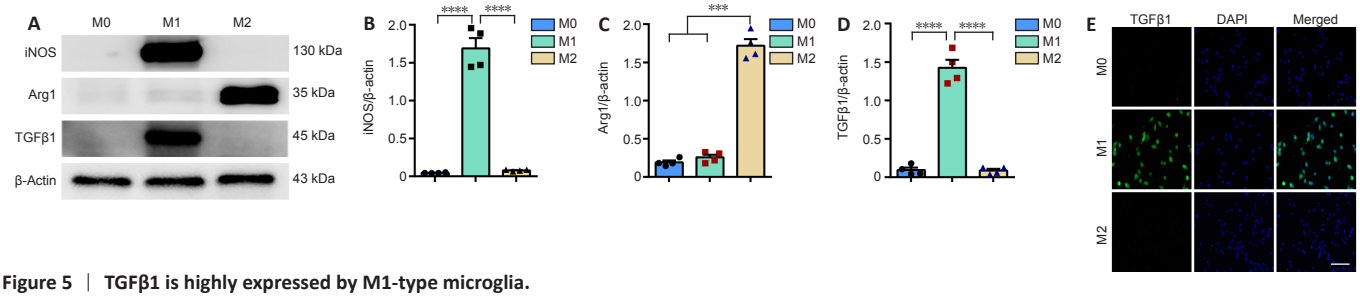

Figure 5 | TGFβ1 is highly expressed by M1-type microglia.
(A) Western blotting shows the expression of M1 (iNOS) or M2 (Arg1) polarization markers and TGFβ1 in BV-2 cells after polarization induction. (B) Quantitative analysis of iNOS expression shown in (A). β-Actin was used as the loading control. iNOS was expressed at significantly higher levels in M1-type microglia than in M0- or M2-type microglia. (C) Quantitative analysis of Arg1 protein expression shown in (A). Arg1 was expressed at significantly higher levels in M2-type microglia than in M0- or M1-type microglia. (D) Quantitative analysis of TGFβ1 protein expression shown in (A). TGFβ1 was expressed at significantly higher levels in M1-type microglia than in M0- or M2-type microglia. The data are presented as the mean ± SEM (n = 4) and were analyzed by one-way analysis of variance, followed by Tukey's *post hoc* test. ***P < 0.001, ****P < 0.0001. (E) Representative immunocytochemistry images of TGFβ1 (green, stained with Alexa Fluor 488) in BV-2 cells after polarization induction. The TGFβ1 fluorescence intensity was strongest in M1-type microglia, suggesting that these cells expressed the highest levels of TGFβ1. DAPI (blue) was used to stain the nuclei. At least three independent replicates were performed for each experiment. Scale bar: 50 μm. Arg1: Arginine 1; DAPI: 4′,6-diamidino-2-phenylindole, dihydrochloride; iNOS: inducible nitric oxide synthase; TGFβ1: transforming growth factor-β1.

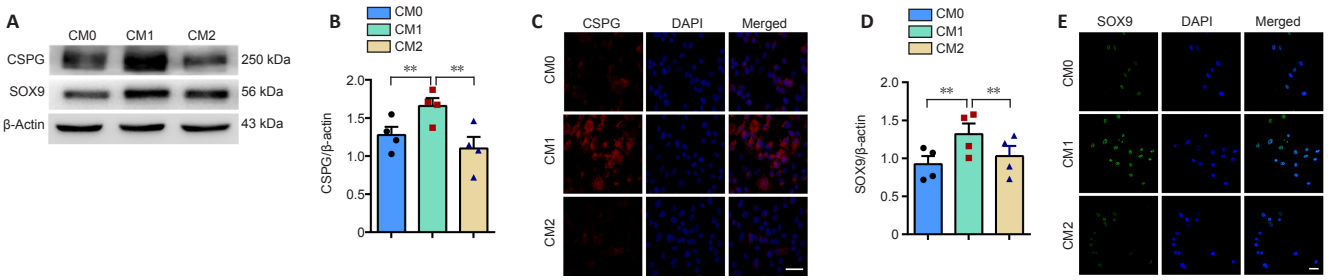

Figure 6 | CM1 induces CSPG production by astrocytes.
(A) Western blot analysis of SOX9 and CSPG expression in C8-D1A cells treated with conditioned media from M0-, M1-, or M2-type microglia (CM0, CM1, or CM2, respectively). (B) Quantitative analysis of CSPG expression shown in A. β-Actin was used as the loading control. CSPG production increased significantly after CM1 treatment. (C) Representative immunofluorescence images of CSPG (red, stained with Alexa Fluor 594) in C8-D1A cells after treatment with conditioned medium. CSPG fluorescence intensity was strongest after CM1 treatment, suggesting that this treatment condition most strongly promoted CSPG production. DAPI (blue) was used to stain the nuclei. Scale bar: 50 μm. (D) Quantitative analysis of SOX9 protein expression shown in A. SOX9 expression increased significantly after CM1 treatment. The data are presented as the mean ± SEM (n = 4). **P < 0.01 (one-way analysis of variance followed by Tukey's *post hoc* test). (E) Representative immunofluorescence images of SOX9 (green, stained with Alexa Fluor 488) in C8-D1A cells treated with conditioned medium. SOX9 fluorescence intensity was strongest after CM1 treatment, suggesting that this treatment condition most strongly promoted SOX9 expression. At least three independent replicates were performed for each experiment. Scale bars: 20 μm in C and E. CM: Conditioned medium; CSPG: chondroitin sulfate proteoglycan; DAPI: 4′,6-diamidino-2-phenylindole, dihydrochloride; SOX9: Sex-determining region Y-box 9.

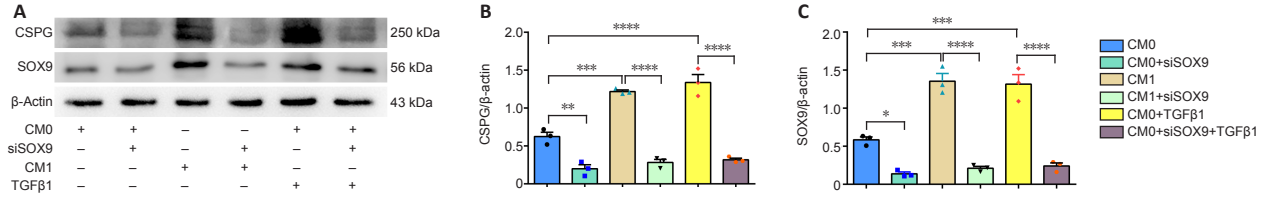

Figure 7 | M1-type microglia induce astrocyte to produce CSPG through the TGFβ1/SOX9 pathway.
(A) Western blot analysis of SOX9 expression and CSPG production in C8-D1A cells after treatment. (B, C) Quantitative analysis of the CSPG production (B) and SOX9 expression (C) shown in (A). β-Actin was used as the loading control. The blots (n = 3) were quantified. The data are presented as the mean ± SEM. *P < 0.05, **P < 0.01, ***P < 0.001, ****P < 0.0001 (one-way analysis of variance followed by Tukey's *post hoc* test). At least three independent replicates were performed for each experiment. CM: Conditioned medium; CSPG: chondroitin sulfate proteoglycan; SOX9: sex-determining region Y-box 9; TGFβ1: transforming growth factor-β1.

SCI can trigger a complex immune response, which includes activation of resident microglia and infiltration of blood-derived macrophages, resulting in an inflammatory response. It is generally believed that neuroinflammation has both advantages and disadvantages for SCI repair, due to differences in immune cell phenotypes and time after injury (David and Kroner, 2011; Miron and Franklin, 2014; Rust and Kaiser, 2017). In previous studies, it was difficult to distinguish between microglia and macrophages after SCI based on morphology and antigenic markers, so they were analyzed collectively as a single microglia/macrophage population (David and Kroner, 2011). These cells can polarize to an M1 or M2 phenotype due to changes in the microenvironment after SCI. Classically activated M1-type microglia/macrophages aggravate tissue injury by producing pro-inflammatory factors (IL-1β, TNFα, IL-6, etc.), proteases, and reactive oxygen species (Miron and Franklin, 2014). In contrast, alternately activated M2-type microglia/macrophages secrete growth-promoting factors (IL-10, IGF-1, etc.) and engulf myelin debris, supporting tissue repair (Ma et al., 2015; Song et al., 2017). However, due to the difficulty of distinguishing microglia from macrophages, microglial polarization after SCI requires further investigation. In recent years, studies using transgenic strategies have shown that CX3CR1, transmembrane protein 119, and purinergic receptor P2Y, G protein coupled 12 are specific markers of microglia (Wang et al., 2015; Bennett et al., 2016; Walker et al., 2020). In the present study, CX3CR1 was used to specifically label microglia after SCI to explore the polarization of microglia rather than macrophages, and showed that microglia primarily exhibited an M1 phenotype at 3 and 7 dpi. Furthermore, we found that M1-type microglia can promote CSPG secretion by astrocytes *in vitro*.

Studies have shown that TGFβ1 can activate TGFβ1 receptor on the surface of astrocytes to increase the transcription of CSPG-related genes via the TGFβ1/mothers against decapentaplegic homolog 2 signal pathway, promoting the deposition of CSPG after brain injury (Schachtrup et al., 2010; Dyck and Karimi-Abdolrezaee, 2015). McKillop et al. (McKillop et al., 2013) found that CSPG deposition is due to SOX9 activation in astrocyte nuclei. Furthermore, TGFβ1 can induce SOX9 pathway activation in astrocytes, while SOX9 inhibition can reduce CSPG deposition (Yuan et al., 2017). Taken together, these findings suggested that the TGFβ1/SOX9 pathway is involved in CSPG deposition, but it remained unclear what cell type produces TGFβ1 and whether the TGFβ1/SOX9 pathway is involved in M1-type microglial regulation of CSPG deposition. In the present study, we found that microglial expression of TGFβ1 increased dramatically after M1 polarization *in vitro*, which was consistent with the high levels of TGFβ1 expression exhibited by microglia *in vivo* at 3 and 7 dpi, when they presented primarily an M1 phenotype. Furthermore, M1-type microglia can induce astrocytes to produce CSPG *in vitro*. To confirm the effect of the TGFβ1/SOX9 pathway on M1-type microglia regulation of CSPG secretion by astrocytes, we designed a rescue experiment and found that, after SOX9 was knocked down in astrocytes, even the addition of TGFβ1 could not rescue the production of CSPG by astrocytes. One limitation of this study is that only a single antibody was used to detect M1/M2 polarization. In future studies, we will use a more systematic approach in the *in vivo* experiments, including the incorporation of additional methods and markers, to further verify our conclusions. Furthermore, it is unlikely that TGFβ1, which is an exocrine cytokine, is the only mediator of crosstalk between microglia and astrocytes, given that the direct contact between microglia and astrocytes suggests that membrane receptors may also play an important role in this process; this possibility requires further investigation.

In conclusion, after SCI, microglia gathered at the lesion border at 14 dpi along the inner border of astrocytic scar. The microglia primarily exhibited an M1 phenotype and expressed high levels of TGFβ1 at 3 and 7 dpi, while at 14 dpi they exhibited primarily an M2 phenotype. Furthermore, we found that M1-type microglia can induce astrocytes to deposit CSPG via the TGFβ1/SOX9 pathway *in vitro*. The findings from the present study may help develop new therapeutic strategies for reducing CSPG deposition, promoting axonal growth, and accelerating functional repair after SCI.

Acknowledgments: *Thanks for the experiment platform provided by the Scientific Research and Experiment Center of the Second Hospital of Anhui Medical University. Thanks to BioRender.com for providing technical support in making graphical abstract.*
Author contributions: *Study design: JHJ, MGZ and SSY; experimental implementation: SSY, ZYL, XZX, and FY; data analysis and figure preparation: YL, and YCL; paper writing: SSY and ZYL; study supervising and paper reviewing: LC, MGZ and JHJ. All authors approved the final version of the manuscript.*
Conflicts of interest: *The authors declare that there are no conflicts of interest associated with this manuscript.*
Financial support: *This work was supported by the National Natural Science Foundation of China, Nos. 81801220 (to MGZ), 81671204 (to JHJ); and Key Research and Development Projects of Anhui Province of China, No. 202004j07020042 (to JHJ). The funding sources had no role in study conception and design, data analysis or interpretation, paper writing or deciding to submit this paper for publication.*
Institutional review board statement: *All the animal procedures were performed in accordance with the guidelines of the Institutional Animal Care and Use Committee of Anhui Medical University (No. LLSC20160052) on March 1, 2016.*
Copyright license agreement: *The Copyright License Agreement has been signed by all authors before publication.*
Data sharing statement: *Datasets analyzed during the current study are available from the corresponding author on reasonable request.*
Plagiarism check: *Checked twice by iThenticate.*
Peer review: *Externally peer reviewed.*

Open peer reviewer: *Jerry Silver, Case Western Reserve University, USA.*
Additional file: *Open peer review report 1.*

References

Alizadeh A, Dyck SM, Karimi-Abdolrezaee S (2019) Traumatic spinal cord injury: an overview of pathophysiology, models and acute injury mechanisms. Front Neurol 10:282.

Allen NJ, Eroglu C (2017) Cell biology of astrocyte-synapse interactions. Neuron 96:697-708.

Alliot F, Pessac B (1984) Astrocytic cell clones derived from established cultures of 8-day postnatal mouse cerebella. Brain Res 306:283-291.

Amor S, Puentes F, Baker D, van der Valk P (2010) Inflammation in neurodegenerative diseases. Immunology 129:154-169.

Anderson MA, O'Shea TM, Burda JE, Ao Y, Barlatey SL, Bernstein AM, Kim JH, James ND, Rogers A, Kato B, Wollenberg AL, Kawaguchi R, Coppola G, Wang C, Deming TJ, He Z, Courtine G, Sofroniew MV (2018) Required growth facilitators propel axon regeneration across complete spinal cord injury. Nature 561:396-400.

Bélanger M, Magistretti PJ (2009) The role of astroglia in neuroprotection. Dialogues Clin Neurosci 11:281-295.

Bellver-Landete V, Bretheau F, Mailhot B, Vallières N, Lessard M, Janelle ME, Vernoux N, Tremblay M, Fuehrmann T, Shoichet MS, Lacroix S (2019) Microglia are an essential component of the neuroprotective scar that forms after spinal cord injury. Nat Commun 10:518.

Bennett ML, Bennett FC, Liddelow SA, Ajami B, Zamanian JL, Fernhoff NB, Mulinyawe SB, Bohlen CJ, Adil A, Tucker A, Weissman IL, Chang EF, Li G, Grant GA, Hayden Gephart MG, Barres BA (2016) New tools for studying microglia in the mouse and human CNS. Proc Natl Acad Sci U S A 113:E1738-1746.

Bradbury EJ, Moon LD, Popat RJ, King VR, Bennett GS, Patel PN, Fawcett JW, McMahon SB (2002) Chondroitinase ABC promotes functional recovery after spinal cord injury. Nature 416:636-640.

Cabezas R, Avila M, Gonzalez J, El-Bachá RS, Báez E, García-Segura LM, Jurado Coronel JC, Capani F, Cardona-Gomez GP, Barreto GE (2014) Astrocytic modulation of blood brain barrier: perspectives on Parkinson's disease. Front Cell Neurosci 8:211.

David S, Kroner A (2011) Repertoire of microglial and macrophage responses after spinal cord injury. Nat Rev Neurosci 12:388-399.

Dyck SM, Karimi-Abdolrezaee S (2015) Chondroitin sulfate proteoglycans: key modulators in the developing and pathologic central nervous system. Exp Neurol 269:169-187.

Elmore MR, Najafi AR, Koike MA, Dagher NN, Spangenberg EE, Rice RA, Kitazawa M, Matusow B, Nguyen H, West BL, Green KN (2014) Colony-stimulating factor 1 receptor signaling is necessary for microglia viability, unmasking a microglia progenitor cell in the adult brain. Neuron 82:380-397.

Faulkner JR, Herrmann JE, Woo MJ, Tansey KE, Doan NB, Sofroniew MV (2004) Reactive astrocytes protect tissue and preserve function after spinal cord injury. J Neurosci 24:2143-2155.

Hara M, Kobayakawa K, Ohkawa Y, Kumamaru H, Yokota K, Saito T, Kijima K, Yoshizaki S, Harimaya K, Nakashima Y, Okada S (2017) Interaction of reactive astrocytes with type I collagen induces astrocytic scar formation through the integrin-N-cadherin pathway after spinal cord injury. Nat Med 23:818-828.

Herz J, Filiano AJ, Smith A, Yogev N, Kipnis J (2017) Myeloid cells in the central nervous system. Immunity 46:943-956.

Hu X, Leak RK, Shi Y, Suenaga J, Gao Y, Zheng P, Chen J (2015) Microglial and macrophage polarization—new prospects for brain repair. Nat Rev Neurol 11:56-64.

Huang DY, Ye M (2012) Microglia and Parkinson's disease. Zhongguo Zuzhi Gongcheng Yanjiu 16:4549-4554.

Jaerve A, Müller HW (2012) Chemokines in CNS injury and repair. Cell Tissue Res 349:229-248.

Joya A, Martín A (2021) Evaluation of glial cell proliferation with non-invasive molecular imaging methods after stroke. Neural Regen Res 16:2209-2210.

Jutzeler CR, Streijger F, Aguilar J, Shortt K, Manouchehri N, Okon E, Hupp M, Curt A, Kwon BK, Kramer JLK (2019) Sensorimotor plasticity after spinal cord injury: a longitudinal and translational study. Ann Clin Transl Neurol 6:68-82.

Kigerl KA, Gensel JC, Ankeny DP, Alexander JK, Donnelly DJ, Popovich PG (2009) Identification of two distinct macrophage subsets with divergent effects causing either neurotoxicity or regeneration in the injured mouse spinal cord. J Neurosci 29:13435-13444.

Kroner A, Greenhalgh AD, Zarruk JG, Passos Dos Santos R, Gaestel M, David S (2014) TNF and increased intracellular iron alter macrophage polarization to a detrimental M1 phenotype in the injured spinal cord. Neuron 83:1098-1116.

Lang BT, Cregg JM, DePaul MA, Tran AP, Xu K, Dyck SM, Madalena KM, Brown BP, Weng YL, Li S, Karimi-Abdolrezaee S, Busch SA, Shen Y, Silver J (2015) Modulation of the proteoglycan receptor PTPσ promotes recovery after spinal cord injury. Nature 518:404-408.

Ma SF, Chen YJ, Zhang JX, Shen L, Wang R, Zhou JS, Hu JG, Lü HZ (2015) Adoptive transfer of M2 macrophages promotes locomotor recovery in adult rats after spinal cord injury. Brain Behav Immun 45:157-170.

McKeon RJ, Höke A, Silver J (1995) Injury-induced proteoglycans inhibit the potential for laminin-mediated axon growth on astrocytic scars. Exp Neurol 136:32-43.

McKeon RJ, Schreiber RC, Rudge JS, Silver J (1991) Reduction of neurite outgrowth in a model of glial scarring following CNS injury is correlated with the expression of inhibitory molecules on reactive astrocytes. J Neurosci 11:3398-3411.

McKillop WM, Dragan M, Schedl A, Brown A (2013) Conditional Sox9 ablation reduces chondroitin sulfate proteoglycan levels and improves motor function following spinal cord injury. Glia 61:164-177.

Miron VE, Franklin RJ (2014) Macrophages and CNS remyelination. J Neurochem 130:165-171.

Miron VE, Boyd A, Zhao JW, Yuen TJ, Ruckh JM, Shadrach JL, van Wijngaarden P, Wagers AJ, Williams A, Franklin RJM, Ffrench-Constant C (2013) M2 microglia and macrophages drive oligodendrocyte differentiation during CNS remyelination. Nat Neurosci 16:1211-1218.

Okada S, Nakamura M, Katoh H, Miyao T, Shimazaki T, Ishii K, Yamane J, Yoshimura A, Iwamoto Y, Toyama Y, Okano H (2006) Conditional ablation of Stat3 or Socs3 discloses a dual role for reactive astrocytes after spinal cord injury. Nat Med 12:829-834.

Orihuela R, McPherson CA, Harry GJ (2016) Microglial M1/M2 polarization and metabolic states. Br J Pharmacol 173:649-665.

Rust R, Kaiser J (2017) Insights into the Dual Role of Inflammation after Spinal Cord Injury. J Neurosci 37:4658-4660.

Schachtrup C, Ryu JK, Helmrick MJ, Vagena E, Galanakis DK, Degen JL, Margolis RU, Akassoglou K (2010) Fibrinogen triggers astrocyte scar formation by promoting the availability of active TGF-beta after vascular damage. J Neurosci 30:5843-5854.

Shen Y, Tenney AP, Busch SA, Horn KP, Cuascut FX, Liu K, He Z, Silver J, Flanagan JG (2009) PTPsigma is a receptor for chondroitin sulfate proteoglycan, an inhibitor of neural regeneration. Science 326:592-596.

Sica A, Mantovani A (2012) Macrophage plasticity and polarization: in vivo veritas. J Clin Invest 122:787-795.

Song JW, Li K, Liang ZW, Dai C, Shen XF, Gong YZ, Wang S, Hu XY, Wang Z (2017) Low-level laser facilitates alternatively activated macrophage/microglia polarization and promotes functional recovery after crush spinal cord injury in rats. Sci Rep 7:620.

Tran AP, Warren PM, Silver J (2018) The biology of regeneration failure and success after spinal cord injury. Physiol Rev 98:881-917.

Van Dyken SJ, Locksley RM (2013) Interleukin-4- and interleukin-13-mediated alternatively activated macrophages: roles in homeostasis and disease. Annu Rev Immunol 31:317-343.

Walker DG, Tang TM, Mendsaikhan A, Tooyama I, Serrano GE, Sue LI, Beach TG, Lue LF (2020) Patterns of expression of purinergic receptor P2RY12, a putative marker for non-activated microglia, in aged and Alzheimer's disease brains. Int J Mol Sci 21:678.

Wang X, Cao K, Sun X, Chen Y, Duan Z, Sun L, Guo L, Bai P, Sun D, Fan J, He X, Young W, Ren Y (2015) Macrophages in spinal cord injury: phenotypic and functional change from exposure to myelin debris. Glia 63:635-651.

Wanner IB, Anderson MA, Song B, Levine J, Fernandez A, Gray-Thompson Z, Ao Y, Sofroniew MV (2013) Glial scar borders are formed by newly proliferated, elongated astrocytes that interact to corral inflammatory and fibrotic cells via STAT3-dependent mechanisms after spinal cord injury. J Neurosci 33:12870-12886.

Yuan J, Liu W, Zhu H, Chen Y, Zhang X, Li L, Chu W, Wen Z, Feng H, Lin J (2017) Curcumin inhibits glial scar formation by suppressing astrocyte-induced inflammation and fibrosis in vitro and in vivo. Brain Res 1655:90-103.

P-Reviewer: Silver J; C-Editor: Zhao M; S-Editors: Yu J, Li CH; L-Editors: Crow E, Yu J, Song LP; T-Editor: Jia Y